Characterisation of silicon sensor materials and designs for the CMS Tracker Upgrade

Alexander DIERLAMM[*][†]

KIT - Karlsruhe Institute of Technology (DE)
E-mail: alexander.dierlamm@cern.ch

During the high luminosity phase of the LHC (HL-LHC, starting around 2020) the inner tracking system of CMS will be exposed to harsher conditions than the current system was designed for. Therefore a new tracker is planned to cope with higher radiation levels and higher occupancies. Within the strip sensor developments of CMS a comparative survey of silicon materials and technologies is being performed in order to identify the baseline material for the future tracker. Hence, a variety of materials (float-zone, magnetic Czochralski and epitaxially grown silicon with thicknesses from 50 μm to 320 μm as p- and n-type) has been processed at one company (Hamamatsu Photonics K.K.), irradiated (proton, neutron and mixed irradiations up to $1.5 \cdot 10^{15} \, \mathrm{n_{eq}/cm^2}$ and beyond) and tested under identical conditions. The wafer layout includes a variety of devices to investigate different aspects of sensor properties like simple diodes, test-structures, small strip sensors and a strip sensor array with varying strip pitch and strip width. This paper presents the current status and results of this campaign.

The 21st International Workshop on Vertex Detectors
16-21 September 2012
Jeju, Korea

---

[*]Speaker.

[†]on behalf of the CMS Tracker Collaboration

1. Introduction

The CMS Tracker Upgrade group conducts an R&D campaign to identify the best silicon material and sensor design for an upgraded silicon strip tracker to be operated during the high luminosity phase of LHC (HL-LHC, starting around 2020). The envisaged integrated luminosity during the high luminosity phase of $3000 \, \text{fb}^{-1}$ is a factor of six larger than the expected integrated luminosity the current detector was designed for [1]. From simulations of the radiation environment at CMS one expects a maximum particle fluence of $1.5 \cdot 10^{15} \, \text{n}_{eq}/\text{cm}^2$ for the silicon strip tracker region [2]. For radiation hardness studies of silicon materials it is also important to note the mixture of particle types, which changes with radius (Fig. 1). Within the RD50[1] collaboration it was found that oxygenated silicon does not follow the NIEL (Non-Ionizing Energy Loss) predictions and a mixture of neutron and charged hadron irradiation could generate compensating defects, which results in an increased charge collection compared to oxygen lean material [3]. Therefore we study sensors made of magnetic Czochralski (MCz; high oxygen concentration due to manufacturing process) and standard float-zone (FZ) material. These sensors are fabricated as n-type devices with p-type strip implants and as p-type devices with n-type strip implants in two versions with p-spray[2] as well as with p-stop[3] strip isolation.

The thinnest silicon sensor in the current tracker is $320 \, \mu\text{m}$ thick. For the Upgrade we investigate thinner sensors ($50 \, \mu\text{m}$ to $320 \, \mu\text{m}$) because of the smaller expected full depletion voltage and leakage current and the reduced material budget. For a currently discussed module type (2S-module [4]) consisting of two strip sensors the difference between $300 \, \mu\text{m}$ and $200 \, \mu\text{m}$ thick silicon makes up about 30% of the total radiation length of the module and therefore also a large fraction of the radiation length of the tracker. The radiation length of the tracking region needs to be kept to a
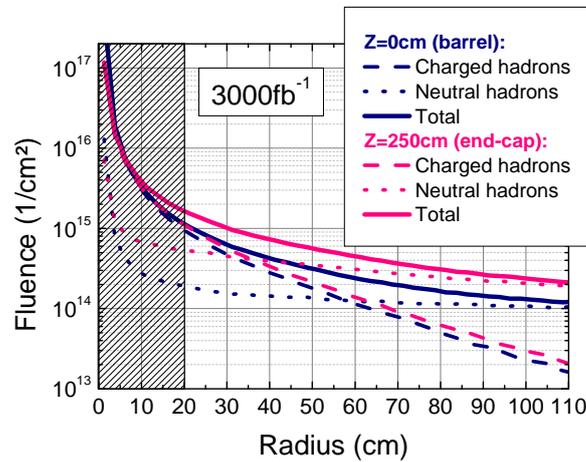
Figure 1: Radial dependence of the particle fluence as simulated by FLUKA for the current CMS tracker layout assuming an integrated luminosity of $3000 \, \text{fb}^{-1}$ (data from [2]). The silicon strip tracker extends from a radius of 20 cm up to 120 cm. The inner region is occupied by the pixel vertex detector.

---

[1] http://rd50.web.cern.ch/rd50/

[2] homogeneous p-type doping layer at moderate peak concentration of about $5 \cdot 10^{15} \, \text{cm}^{-3}$

[3] structured p-type implantation with higher peak concentration ($> 2 \cdot 10^{16} \, \text{cm}^{-3}$) surrounding the strip implants
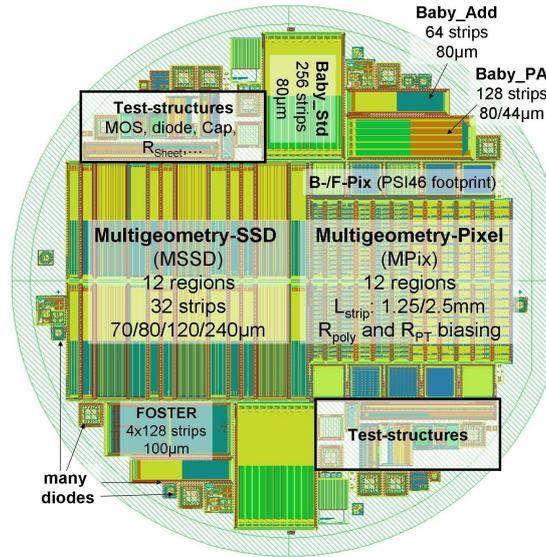
Figure 2: The layout of the R&D wafer with many devices. Diodes and mini-strip sensors (Baby_Std, Baby_Add), multi-geometry strip sensor (MSSD), test-structures (TS), a mini-strip sensor with integrated pitch-adapter (Baby_PA), a four-fold segmented strip sensor with edge read-out (FOSTER) and a multi-geometry pixel structure (MPix).

minimum to avoid photon conversions, nuclear interactions and multiple-scattering.

Another aspect of the sensor R&D is the investigation of layout variations. One obvious parameter is the strip pitch, which has an impact on the strip capacitance, which in turn significantly affects the sensor noise. As mentioned before, we also study the implication of strip isolation techniques, not only on these devices, but also with other manufacturers and by T-CAD simulations [5, 6]. Further more, we investigate the influence of routing lines connecting the charge sensitive strip implants to the pads for wire bonding to the read-out chips. This can be used to spare the commonly used additional glass pitch-adapter by implementing the pitch-adapter on the sensor itself. Another application is the connection of sensitive regions in the centre of the sensor to the outer edge for a more convenient connection to the read-out chips as needed for the 2S-module concept [4].

All these aspects are addressed by one big irradiation and measurement campaign within the CMS Tracker Upgrade group. We have designed one single mask layout, which comprises several different devices for the individual purposes (Fig. 2):

Diodes Evaluation of generated defects. IV[4] and CV[5] measurements, Transient Current Technique (TCT) [7] and edge-TCT measurements to extract the charge collection efficiency (CCE), trapping and electric fields. Thermally Stimulated Current and Deep Level Transient Spectroscopy to investigate defect characteristics.

Mini-strip sensors Evaluation of radiation hardness of the different materials. IV and CV measurements, strip characterisation, charge collection measurements (results presented in this paper) and Lorentz Angle measurements [8].

---

[4]current vs. voltage characteristic

[5]total capacitance vs. voltage characteristic

Multi-geometry strip sensors Evaluation of strip sensor properties for a variation of strip pitches and width-to-pitch ratios. Also used for beam test analysis [9].

Multi-geometry pixel sensors Characterisation of a sensor with very short strips (1-2mm), varying pitch and biasing connection (poly-silicon or punch-through) [10].

Test-structures Characterisation of the process quality [11].

Advanced designs Evaluate the performance of a strip sensor with integrated pitch-adapters and a four-fold segmented strip sensor with edge read-out . Furthermore there are pixel sensors with layout variations which fit the current CMS pixel read-out chip (PSI46) footprint.

This layout has been processed on different wafer materials (FZ: 320 µm, 200 µm, 120 µm; MCz: 200 µm; Epi: 100 µm, 50 µm; all as n- and p-type with p-stop or p-spray) by one manufacturer (Hamamatsu Photonics K.K.) for best comparability of the results. This manufacturer was selected due to the known very good quality and the capability to produce the quantity needed for a large scale production for a new tracker.

Labels for the materials discussed in this paper are composed of silicon type (FZ: float-zone with physical thickness of 320 µm and deep diffusion to eventually reduce the active thickness; M: magnetic Czochralski (MCz); FTH: thinned float-zone), nominal active thickness (320, 200) and doping type (N: n-type; P: p-type with p-stop; Y: p-type with p-spray).

The samples have been characterised in detail after production and went through selected irradiations with protons and neutrons (Tab. 1). The fluences are selected to reflect the conditions in the tracker in view of total fluence and mixture of charged and neutral particles for a few radii under study as depicted in Fig. 1. Irradiations are performed with 23 MeV protons at ZAG[6], Germany, and reactor neutrons in Ljubljana[7], Slovenia. We chose protons as charged particles although the main contribution at LHC comes from pions, since the known proton sources deliver the necessary higher fluxes, are more easily accessible, and [12] showed that there were no significant differences

Table 1: Summary of the foreseen particle fluences for this campaign. The values represent regions inside the tracker volume at the given positions. They were chosen such that we also take increasing neutron fluences to study the effects of increasing pure neutron irradiation. **Bold** numbers indicate irradiations covered in this paper, roman numbers indicate irradiations in progress and *italic* numbers represent planned irradiations for the pixel region.

Radius	z-Position	Protons	Neutrons	Total	Ratio p/n
cm	cm	$10^{14}\,\mathrm{n_{eq}cm^{-2}}$	$10^{14}\,\mathrm{n_{eq}cm^{-2}}$	$10^{14}\,\mathrm{n_{eq}cm^{-2}}$	
40	**250**	**3**	**4**	**7**	**0.75**
20	**250**	**10**	**5**	**15**	**2.0**
15	250	15	6	21	2.5
10	*255*	*30*	*7*	*37*	*4.3*
5	*260*	*130*	*10*	*140*	*13*

4
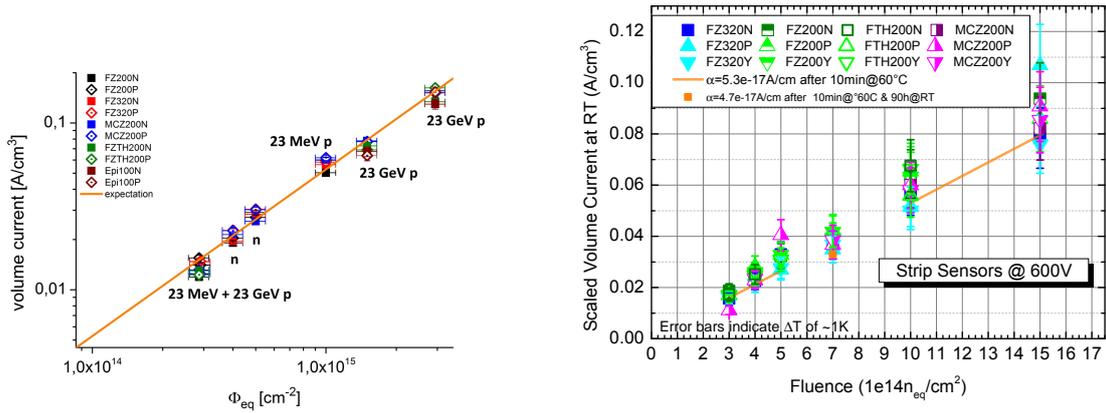
(a) Volume generated leakage current of diodes at a bias voltage 5% above full depletion voltage [7]. Currents have been measured at 0°C and scaled to +20°C according to [14]. Various particle types have been used for these irradiation of single particle type (as indicated).

(b) Leakage current of strip sensors at 600 V for all materials measured at -20°C and scaled to +20°C according to [14].

Figure 3: Leakage currents of diodes and mini-strip sensors after annealing of 10 min at 60°C. The expectations follow the parametrisation derived from many measurements in [13].

in charge collection when comparing protons with pions on FZ silicon. During the campaign we decided to add further irradiations with 800 MeV and 23 GeV protons to check the dependence on the particle energy. These evaluations are ongoing and not subject of this paper.

This paper presents the measurements on mini-strip sensors performed and analysed so far.

2. Leakage current and full depletion voltage

The most basic properties of a silicon sensor are its leakage current and full depletion voltage. The increase of leakage current in diodes with irradiation fluence is well studied and follows a single parametrisation independent of particle type and energy or sensor material [13]. Therefore this measurement can serve as a standard to confirm irradiation fluences. In this campaign, diodes have been irradiated together with all the other devices to the same fluence where possible. The measured volume generated leakage currents of diodes (Fig. 3(a)) confirm the expectations and demonstrate the independence of silicon material and particle type. It also indicates that the target fluences are met for all devices within a group. For mini-strip sensors (Fig. 3(b)) we measure an excess current compared to the expectation for most of the samples up to about 40%. The IV curves (an example is shown in Fig. 4(a)) of the mini-strip sensors do not show saturation above the full depletion voltage as it is observed for diodes. Therefore we plot the leakage currents at a fixed voltage of 600 V, which is the highest voltage the tracker power supplies can currently deliver. With this approach we can get an estimation of the expected currents during the operation of the strip sensors in the experiment. For example, a sensor at 40 cm radius would receive a fluence of about $5 \cdot 10^{14}\,\mathrm{n_{eq}/cm^2}$. The measurements of our mini-strip sensors (volume of $0.149\,\mathrm{cm^3}$) yield about 90 μA at -20°C at that fluence. Scaling to the foreseen sensor size (10 cm×10 cm, 200 μm thick) the leakage current results in 1.2 mA and therefore a heating power of 0.7 W at 600 V per sensor, which

(a) Total leakage current vs. bias voltage.

(b) Total sensor capacitance vs. bias voltage.
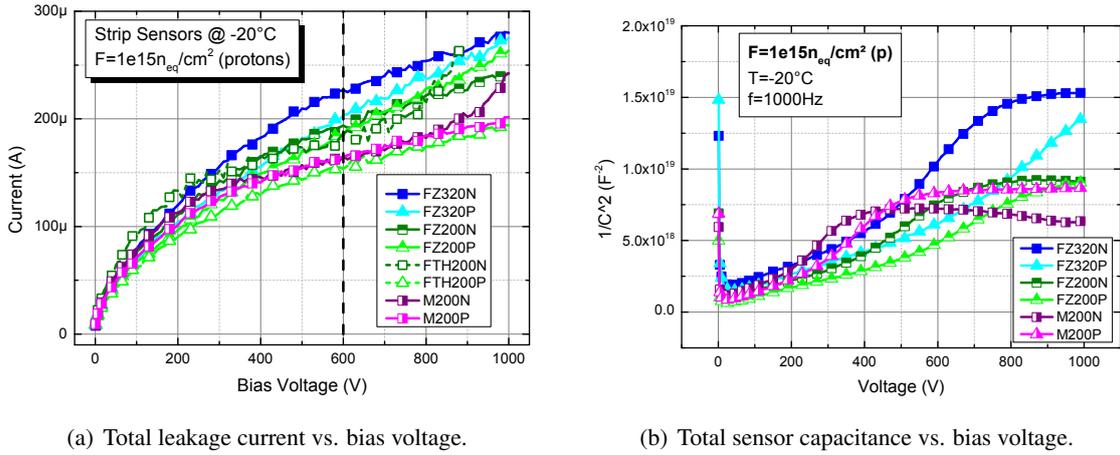
Figure 4: Examples of IV and CV curves after $1 \cdot 10^{15}\,n_{eq}/cm^2$ at -20°C.

(a) Full depletion voltages vs. fluence.

(b) Effective doping concentration (N_{eff}) for diodes and strip sensors vs. fluence.
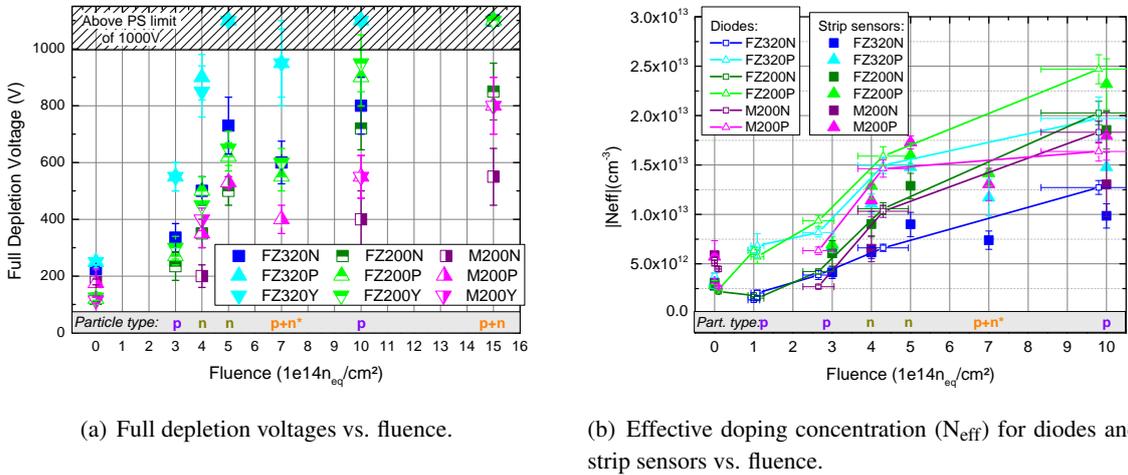
Figure 5: Full depletion voltage of mini-strip sensors as extracted from CV-curves at -20°C and 1 kHz. Sensors at $7 \cdot 10^{14}\,n_{eq}/cm^2$ indicated by 'p+n*' have been exposed to about four days longer annealing at room temperature than all other measurements, which were annealed for 10 min at 60°C after each irradiation (details in [15]). The N_{eff} is calculated from the extracted full depletion voltage and, for strip sensors, corrected for the effects by segmentation [16].

needs to be evacuated. Keeping in mind that there might be longer annealing times than applied for these measurements, the stated power would be an upper limit, since leakage current drops with annealing time [13].

The full depletion voltage is extracted from the capacitance-voltage characteristic of the sensors by plotting $1/C^2$ over bias voltage and identifying the turnover to saturation. This method works well for non-irradiated sensors, but is not very accurate for irradiated sensors, since no sharp transition is observed (an example is given in Fig. 4(b)). Figure 5(a) shows the full depletion voltages for the various materials and particle fluences. These measurements confirm that the sensor thickness increases the full depletion voltage and that a p-type sensor has higher full depletion voltage than the n-type version of the same thickness after irradiation. This is due to the donor concentration

in n-type sensors, which compensates part of the generated acceptor-like defects [13]. Further we observe in Fig. 5(a) different slopes for neutron- and proton-only irradiated samples (steeper for neutron irradiations), and that MCz material has lower full depletion voltage than FZ material with the same thickness of about 200 μm. In Fig. 5(b) the calculated effective doping concentration of mini-strip sensors are confirmed by measurements on diodes. Only for M200N at $1 \cdot 10^{15}\,\mathrm{n_{eq}/cm^2}$ the extracted full depletion voltage seems to be too low compared to the diode measurements and compared to the charge collection measurements in Sec. 4. This demonstrates the potential inaccuracy of the method for CV curves as in Fig. 4(b).

Further irradiations representing the 15 cm radius in Tab. 1 are currently in progress and should give a clearer picture.

3. Strip characteristics

The quality and performance of an AC coupled strip sensor is not only characterised by leakage current and full depletion voltage but also by the strip characteristics like coupling capacitance, bias resistance, inter-strip resistance and inter-strip capacitance. In addition, we also check for pinholes, which are shorts between the strip implant and the metal read-out strip through the coupling oxide. In this campaign we did not find a single one, which underlines the excellent quality of the devices.

Fig. 6 summarizes the strip parameter measurements (bias resistance, inter-strip resistance, coupling capacitance and inter-strip capacitance) for all materials and their development over fluence. The value of the poly-silicon bias resistance (Fig. 6(a)) strongly depends on processing details and can vary from wafer to wafer. Values in the range from 1 MΩ to 4 MΩ are acceptable as long as the resistance is lower than the inter-strip resistance, but higher than the strip implant resistance. Homogeneity of the resistance over the sensor is much more important and the standard deviation should be less than 10%. On these devices we measured a typical standard deviation of less than 1.5% [15]. At the lowest fluence point we see an increase of the bias resistance of about 10%, which more or less stays at that level also for higher fluences.

The inter-strip resistance (Fig. 6(b)), in contrary, strongly depends on the irradiation fluence. Initial resistances of more than 100 GΩcm fall below 1 GΩcm after a fluence of $1 \cdot 10^{15}\,\mathrm{n_{eq}/cm^2}$. However, this value is still high enough to isolate the strips from each other. This is especially interesting for the p-type sensors with p-spray isolation, which require a well optimized process [17]. For FZ320Y we have an additional data point at $3.8 \cdot 10^{15}\,\mathrm{n_{eq}/cm^2}$, which has still a high inter-strip resistance value of more than 50 MΩcm. Additional signal measurements on this sensor also show well defined clusters, which means that the isolation is sufficient. From this we can conclude that HPK manages to process a p-spray isolation with a sufficiently high break-down voltage and good isolation capability.

The coupling capacitance (Fig. 6(c)) varies within about 4%, which is a rather small effect, and hence negligible for operation.

Changes of the inter-strip capacitance (Fig. 6(d)) directly affect the strip capacitance and therefore the read-out noise. After an initial increase of about 5% after $3 \cdot 10^{14}\,\mathrm{n_{eq}/cm^2}$ for most of the materials it stays flat over fluence. Only the data point of FZ320Y at the highest fluence of $3.8 \cdot 10^{15}\,\mathrm{n_{eq}/cm^2}$ is reduced again, which could be related to the low inter-strip resistance.
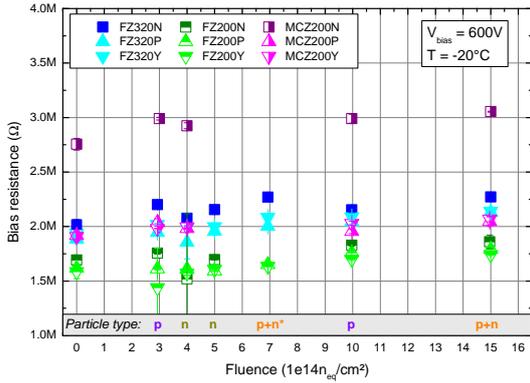
(a) Bias resistance. Measurements before irradiation have been taken at +20°C and scaled up by 16% as measured in [15].
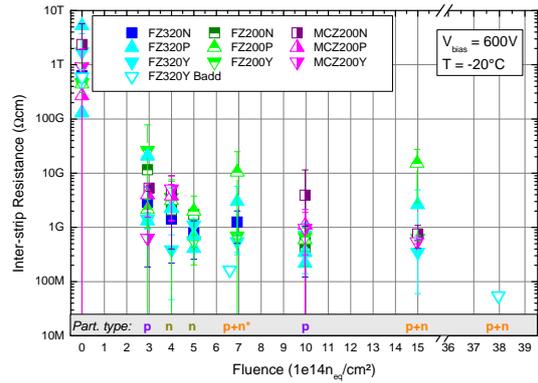
(b) Inter-strip resistance per length. Data points labelled FZ320Y Badd were measured on a smaller sensor with same strip pitch and width, but at −10°C, which results in lower values.
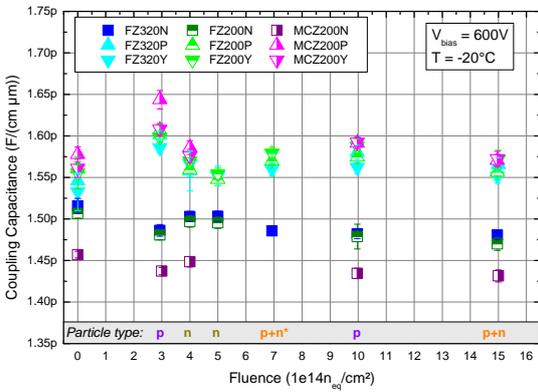
(c) Coupling capacitance per length and width of implant.
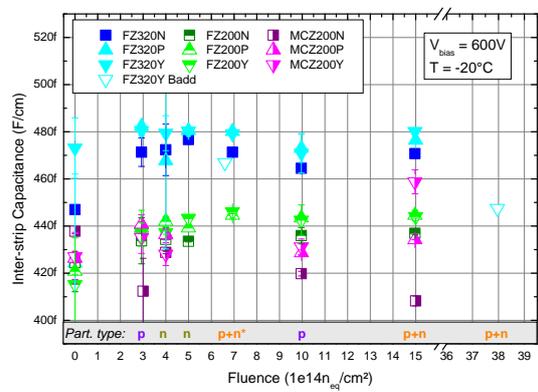
(d) Inter-strip capacitance per length as measured to one neighbour.

Figure 6: Overview of relevant strip characteristics measured at −20°C and 600V reverse bias voltage, if not stated otherwise.

4. Charge collection

The signal to noise ratio is the most important parameter for hit identification. Parameters which affect the noise, like leakage current and capacitances, have already been discussed. The collected charge forms the signal and depends on bias voltage and fluence as shown in Fig. 7. These measurements have been performed with a Sr90 source and an ALiBaVa analogue read-out system [18]. The signals have been calibrated assuming the charge generation of the primary electrons to be $80e^-/\mu m$. The gain of the chips is temperature dependent and different for each chip. This was considered and corrected to about 5% accuracy [19].

The initially higher signal of the thick materials (Fig. 7) drops fast with increasing fluence until it reaches the charge collection of the thin materials at about $1 \cdot 10^{15} \, n_{eq}/cm^2$. At that fluence and between 300V and 600V the physically thin materials (M and FTH) collect more charge than the thick sensors (Fig. 8(a)). This effect is most pronounced for MCz material, which also has the low-
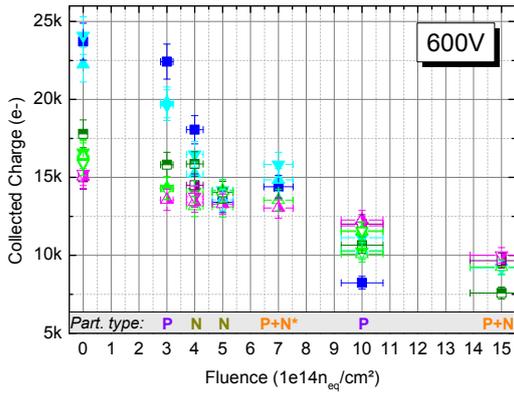
(a) Charge collection at a reverse bias voltage of 600 V.
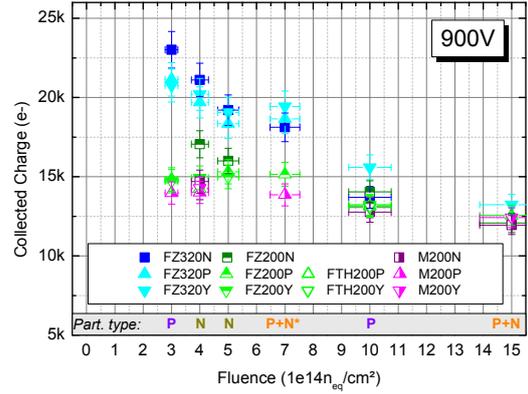
(b) Charge collection at a reverse bias voltage of 900 V.

Figure 7: Charge collection vs. irradiation fluence. Measurements have been taken at $-20\,^{\circ}\mathrm{C}$ with a Sr90 source and an ALiBaVa read-out system after 10 min at $60\,^{\circ}\mathrm{C}$ (sensors at $7 \cdot 10^{14}\,\mathrm{n_{eq}/cm^2}$ after additional 90 h at room temperature and sensors at $1.5 \cdot 10^{15}\,\mathrm{n_{eq}/cm^2}$ after 20 min at $60\,^{\circ}\mathrm{C}$). A cluster has a seed signal $>5\times$ strip noise and neighbours of $>2\times$ strip noise.
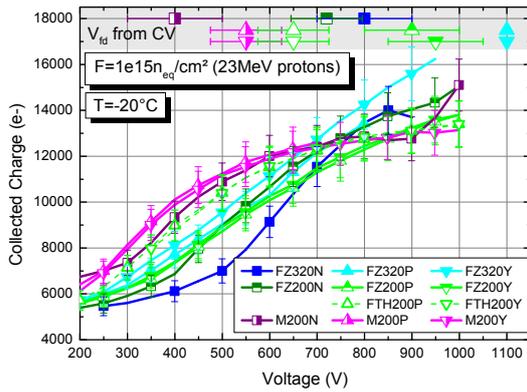
(a) Collected charge vs. voltage after $1 \cdot 10^{15}\,\mathrm{n_{eq}/cm^2}$ 23 MeV protons and annealing of 10 min at $60\,^{\circ}\mathrm{C}$.
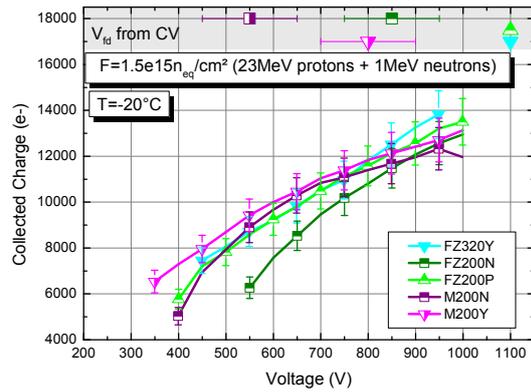
(b) Collected charge vs. voltage after $1.5 \cdot 10^{15}\,\mathrm{n_{eq}/cm^2}$ 23 MeV protons and 1 MeV neutrons mixed and annealing of about 20 min at $60\,^{\circ}\mathrm{C}$.

Figure 8: Charge collection vs. bias voltage at $-20\,^{\circ}\mathrm{C}$. In the upper shaded area the estimated full depletion voltages from CV curves are given.

est full depletion voltages. Both plots in Fig. 8 demonstrate that at these fluences the full depletion voltage is still a good indication of the needed bias voltage to get at least about 90% of the maximum charge (below 1000 V). Only outlier is M200N, for which the slightly distorted CV curve led to a wrong extraction of the full depletion voltage (Fig. 4(b)). Still, the sensors collect reasonable charge above $10\,\mathrm{ke^-}$ even below full depletion voltage.

At 900 V (Figs. 7(b) and 8) most of the investigated materials become comparable in terms of charge collection both after $1 \cdot 10^{15}\,\mathrm{n_{eq}/cm^2}$ proton irradiation and $1.5 \cdot 10^{15}\,\mathrm{n_{eq}/cm^2}$ mixed irradiation. The collected charge of around $12.5\,\mathrm{ke^-}$ is slightly lower than stated in [12] ($13\,\mathrm{ke^-}$ to $15\,\mathrm{ke^-}$ for 300 μm p-type FZ sensors), but reasonably close given that the annealing state could be
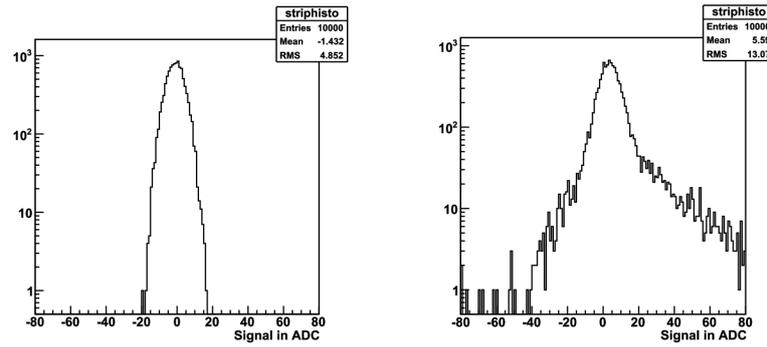
(a) Randomly triggered signal distribution at 600V.

(b) Randomly triggered signal distribution at 900V.

Figure 9: Example of observed non-Gaussian noise of highly irradiated n-type sensors (FZ320N, FZ200N and M200N). These plots show the pedestal subtracted signal distribution (log-scale) of a M200N sensor after $1.5 \cdot 10^{15} \, n_{eq}/cm^2$ mixed irradiation and about 13 days of equivalent annealing at room temperature.
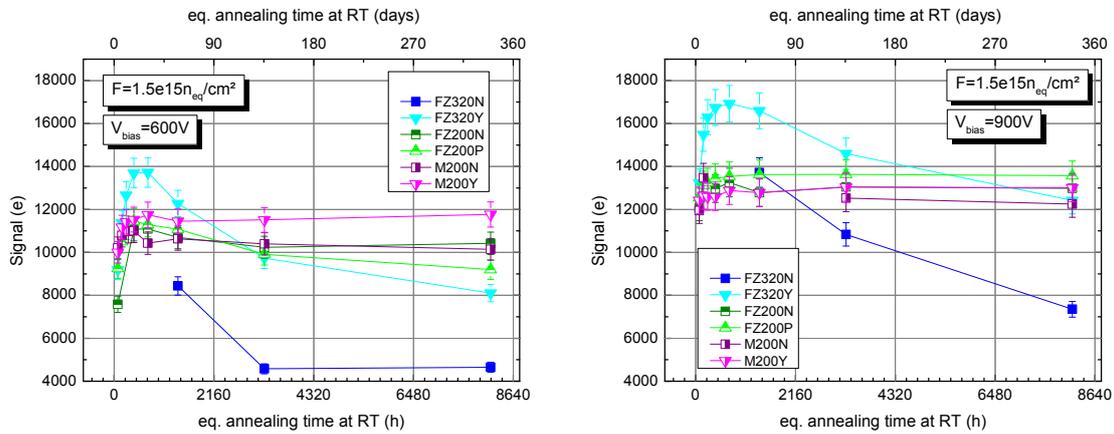
(a) Charge collection at a reverse bias voltage of 600 V.

(b) Charge collection at a reverse bias voltage of 900 V.

Figure 10: Annealing of charge collection for the highest expected fluence of the strip sensor region in the tracker. Thin materials at high bias voltage deliver a constant charge of above $12 \, ke^-$ after a small initial increase shortly after irradiation. The annealing is performed at $60\,^\circ C$ (for 20, 20, 40 and 75 min) and then at $80\,^\circ C$ (for 15, 30 and 60 min). The indicated duration is scaled to annealing at room temperature by the scaling of leakage current annealing from [13].

different.

An exception is FZ320N at $1.5 \cdot 10^{15} \, n_{eq}/cm^2$. For this material and fluence we cannot detect a signal at moderate voltages, and with increasing bias voltage we get increasing non-Gaussian noise contributions, which makes an operation impossible (also observed for measurements on an MSSD in a beam test and Baby_add during Lorentz angle measurements). This effect of increasing irreducible non-Gaussian noise, which might originate from micro-discharges, is also observed considerably on M200N and less severe on FZ200N after some annealing of about 10 days (Fig. 9). After longer annealing of about 90 days the noise is going down again. p-type materials seem not to be affected though.

The annealing of the charge collection is shown in Fig. 10 for the highest fluence point. An initial beneficial annealing of the signal is clearly visible at 600 V, which reaches a maximum of the charge collection after about 20 days. Thick materials show a continuing decrease of the charge collection with annealing time, which has to be taken into account for planning of maintenance periods without cooling. Thin materials at high voltages don't show a decrease of charge collection with longer annealing time, therefore one could profit from annealing of the leakage current to reduce the noise resulting in an increase of the signal to noise ratio.

5. Summary and Outlook

The foreseen measurements are not completed yet, which does not allow a final conclusion. We still miss most measurements from samples irradiated with 23 GeV and 800 MeV protons and further irradiation steps corresponding to smaller radii (Tab. 1) to investigate materials for the pixel region and to study contingencies for the strip sensors.
Preliminary conclusions for strip sensor measurements up to $1.5 \cdot 10^{15} \, \mathrm{n_{eq}/cm^2}$ are:

- Leakage currents of strip sensors can be about 40% higher than expected from diode measurements due to surface currents and/or charge multiplication in the high field regions around the strips.

- The extracted full depletion voltage from CV curves is still a good indication for the minimum bias voltage to be applied to exploit the potential charge collection.

- All characteristic strip parameters, except inter-strip resistance and of course strip leakage currents, are only moderately changed with irradiation. Even the initially fast decreasing inter-strip resistance seems to saturate at higher fluences staying at a level which is sufficient to isolate the strips for both p-stop and p-spray technologies of HPK.

- After an irradiation equivalent to a radius of 40 cm the collected charge at 600 V is sufficient ($>13 \mathrm{ke^-}$) for all investigated materials. At 900 V, the 320 μm sensors collect about $5 \mathrm{ke^-}$ more charge than the 200 μm thick ones.

- After an irradiation equivalent to a radius of 20 cm the collected charge at 600 V is small ($<10 \mathrm{ke^-}$) for all investigated materials and inefficiencies might occur depending on the readout electronics. Applying 900 V increases the collected charge above $12 \mathrm{ke^-}$ for most of the materials but FZ320N, for which we do not see a signal at all. During the annealing phase M200N and FZ200N show irreducible non-Gaussian noise, which does not allow proper hit identification.

- After an initial small increase of collected charge with annealing time the charge stays constant over one year at room temperature for thin 200 μm devices. Thick p-type sensors allow to collect up to 25% more charge during a beneficial annealing phase, but approach the charge collection of thin sensors after one year.

Now we are beginning to study implications of the measured sensor properties on a binary readout and on the discrimination concept as described in [4]. This should allow us, together with the

additional measurements, to conclude on the baseline sensor material for the CMS Tracker Upgrade by spring 2013. This process will also include simulation studies of the overall performance of a future tracker with the selected material and consider aspects of costs and material budget.

Acknowledgments

References

[1] CMS Collaboration, *CMS Tracker Technical Design Report*, 1998, CERN/LHCC 98-6.

[2] S. Müller, *The Beam Condition Monitor 2 and the Radiation Environment of the CMS Detector at the LHC*, 2010, CMS-TS-2010-042.

[3] G. Casse, *Overview of the recent activities of the RD50 collaboration on radiation hardening of semiconductor detectors for the sLHC*, *NIM A* **598**, 2009, pp. 54-60.

[4] D. Abbaneo, *Upgrade of the CMS Tracker with tracking trigger*, 2011, *JINST* **6** C12065.

[5] Th. Eichhorn, *Silicon Strip Sensor Simulations for the CMS Phase-II Tracker Upgrade*, 2012, CMS CR-2012/320, presented at IEEE-NSS-MIC-RTDS2012.

[6] M. Strelzyk, *Design studies of n-in-p silicon strip sensors for the CMS Tracker*, *diploma thesis*, 2012, Karlsruhe Intitute of Technology, IEKP-KA/2012-022.

[7] G. Steinbrück, *Towards Radiation Hard Sensor Materials for the CMS Tracker Upgrade*, 2012, CMS CR-2012/308, presented at IEEE-NSS-MIC-RTDS2012.

[8] A. Nürnberg, *Lorentz angle measurements as part of the sensor R&D for the CMS Tracker upgrade*, 2012, presented at iWoRID in Figueira da Foz, approved by JINST, JINST_033P_0912.

[9] G. Auzinger, *Analysis of Testbeam Data of Irradiated R&D Sensors for the CMS Tracker Upgrade*, 2012, presented at RESMDD in Florence, to be published in NIM A.

[10] M. Bergholz, *Radiation hard sensor materials for the CMS tracker upgrade*, 2011, CMS CR-2011/308 and IEEE-NSS-MIC2011 [doi:10.1109/NSSMIC.2011.6154463].

[11] B. Lutzer, *Characterization of irradiated test structures for the CMS tracker upgrade*, 2012, presented at RESMDD in Florence, to be published in NIM A.

[12] A. Affolder et al., *Collected charge of planar silicon detectors after pion and proton irradiations up to $2.2 \cdot 10^{16}$ n_{eq}/cm^2*, *NIM A* **623**, 2010, p. 177.

[13] M. Moll, *Radiation Damage in Silicon Particle Detectors*, *phd thesis*, University of Hamburg, 1999, desy-thesis-99-040.

[14] A. Chilingarov, *Generation current temperature scaling* , RD50 Technical Note RD50-2011-01 [http://rd50.web.cern.ch/rd50/doc/Internal/rd50_2011_001-I-T_scaling.pdf].

[15] K.-H. Hoffmann, *Development of New Sensor Designs and Investigations on Radiation Hard Silicon Strip Sensors for the CMS Tracker Upgrade at the High Luminosity Large Hadron Collider*, *phd thesis*, 2013, Karlsruhe Intitute of Technology, IEKP-KA/2013-1.

[16] E. Barberis et al., *Capacitances in silicon microstrip detectors*, *NIM A* **342**, 1994, p.90.

[17] G. Pellegrini et al., *Technology of p-type microstrip detectors with radiation hard p-spray, p-stop and moderated p-spray insulations*, *NIM A* **579** (2007), p. 599.

[18] R. Marco-Hernández et al., *A Portable Readout System for Microstrip Silicon Sensors (ALIBAVA)*, *IEEE Transactions on Nuclear Science* **56(3)**, 2009, p. 1642.

[19] S. Frech, *Einfluss von Strahlenschäden auf Siliziumstreifensensoren aus unterschiedlichen Grundmaterialien*, *diploma thesis*, 2012, Karlsruhe Intitute of Technology, IEKP-KA/2012-021.

[20] M. Raymond and G. Hall, *CMS Microstrip Tracker Readout at the SLHC*, *Proceedings of Topical Workshop on Electronics for Particle Physics*, 2008, CERN-2008-008, p. 354.

[21] G. Hall, *Conceptual study of a trigger module for the CMS Tracker at SLHC*, *NIM A* **636**, 2011, pp. S201-S207.